# Hypersingular integral equation based micromechanical models for a microscopically damaged antiplane interface between a thin elastic layer and an elastic half space+

X. Wang, W. T. Ang* and H. Fan
School of Mechanical and Aerospace Engineering
Nanyang Technological University
Singapore 639798

**Abstract**

Two micromechanical models based on the hypersingular integral formulations are presented for estimating the effective stiffness of a micro-cracked interface between a thin elastic layer and an elastic half space under antiplane deformations. The three-phase model simplifies the interface into three parts − micro-cracked, perfectly bonded and effective regions. The micromechanical-statistical model takes into consideration statistical variations in the lengths of randomly positioned interfacial micro-cracks. Some parametric studies are carried out on how the plane boundary of the thin layer and the material properties of the thin layer and the half space affect the effective stiffness of the interface.

*Keywords*: Micromechanics, microscopically damaged interface, effective stiffness, thin film, hypersingular integral equations.

+ Article published in *Applied Mathematical Modelling*
http://dx.doi.org/10.1016/j.apm.2015.02.002
* Author for correspondence

# 1 Introduction

Thin film structures form the basic components of many microelectronic devices. They exists in almost all essential elements of integrated circuit technology, such as microprocessor and electrical actuators. As explained in Nix [8], a thin film may be formed by coating at a very high temperature a layer of material on a substrate of a different material. During the cooling process, the mismatch of the thermal expansion coefficient between the layer and the substrate may give rise to thermally induced residual stresses, resulting in the formation of interfacial micro-defects. Thus, the analysis of damaged interfaces between the thin layer and the substrate is of considerable importance in assessing the reliability of microelectronic devices (see, for example, Suo and Hutchinson [9], Varias, Mastorakos and Aifantis [10] and Xu, Blume and Shih [12]).

A microscopically damaged interface may be modeled as containing interfacial micro-cracks. For macro-level mechanics, the micro-cracked interface may be regarded as a continuous distribution of springs with an effective stiffness to be estimated by taking into consideration some microscopic details of the interface. Fan and Sze [6] presented a three-phase model for estimating the effective electric property of the interface between two dielectric half spaces and employed the finite element method to solve approximately the boundary value problem for the model. More recently, Wang, Ang and Fan [11] proposed a micromechanical model for calculating the interface effective stiffness between two anisotropic elastic half spaces under antiplane shear loads, allowing for statistical variations in the lengths of randomly positioned interfacial micro-cracks. If the variation in the lengths of the micro-cracks is small and if the micro-cracks are more or less evenly distributed on the interface, the value of effective stiffness estimated by the micromechanical-

statistical model in [11] is found to be close to that given by the corresponding three-phase model of the interface.

The micromechanical-statistical and the three-phase models in [11] are formulated and solved in terms of hypersingular integral equations. An advantage of the hypersingular integral formulations is that the unknown functions on the micro-cracks are the crack-opening displacements (Ang [2]). Once the hypersingular integral equations are solved, the interface effective stiffness, which is related to the displacement jump across the interface in the macro spring model, can be easily computed. Furthermore, the numerical solution of the integral equations does not require the use of any artificially introduced boundary for the elastic half spaces.

In the present paper, the hypersingular boundary integral equation based models in [11] are extended to estimate the effective stiffness of a micro-cracked interface between a thin elastic layer and an elastic half space under antiplane deformations. Some parametric studies are carried out using the micromechanical-statistical model to investigate how the plane boundary of the thin layer and the material properties of the thin layer and the half space affect the effective stiffness of the interface.

# 2 The problem

Referring to a Cartesian coordinate frame $Ox_1x_2x_3$, consider a thin homogeneous anisotropic elastic layer occupying the region $0 < x_2 < h$. The layer is bonded to a homogeneous anisotropic elastic half space in the region $x_2 < 0$. The interface between the thin elastic layer and the elastic half space is microscopically damaged with interfacial micro-cracks.

The bimaterial is assumed to be undergo an antiplane elastostatic deformation. The only non-zero component of the elastic displacement, denoted

by $u_3$, is the one along the $x_3$ direction and varies with only the spatial coordinates $x_1$ and $x_2$. The antiplane components of the stress are given by

$$\sigma_{3i} = \lambda_{ij}(x_1, x_2)\frac{\partial u_3}{\partial x_j}, \tag{1}$$

where $\lambda_{ij}$ are elastic coefficients defined by

$$\lambda_{ij}(x_1, x_2) = \begin{cases} \lambda_{ij}^{(1)} & \text{for } 0 < x_2 < h, \\ \lambda_{ij}^{(2)} & \text{for } x_2 < 0, \end{cases} \tag{2}$$

with $\lambda_{ij}^{(p)}$ being positive constants such that $\lambda_{ij}^{(p)} = \lambda_{ji}^{(p)}$ and $(\lambda_{12}^{(p)})^2 - \lambda_{11}^{(p)}\lambda_{22}^{(p)} < 0$. Note that the Einsteinian convention of summing over a repeated index holds here for Latin subscripts which take the values 1 and 2.

From (1) and the equilibrium equations of elastostatics, $u_3$ is required to satisfy the partial differential equation

$$\frac{\partial}{\partial x_i}(\lambda_{ij}\frac{\partial u_3}{\partial x_j}) = 0. \tag{3}$$

The antiplane displacement $u_3$ and stress $\sigma_{3i}$ along a macroscopic portion of the microscopically damaged interface $x_2 = 0$ may be homogenized by using the averaging procedure

$$\begin{aligned} \widehat{u}_3(\widehat{x}_1, 0^{\pm}) &= \frac{1}{2\ell}\int_{\widehat{x}_1-\ell}^{\widehat{x}_1+\ell} u_3(x_1, 0^{\pm})dx_1, \\ \widehat{\sigma}_{3i}(\widehat{x}_1, 0^{\pm}) &= \frac{1}{2\ell}\int_{\widehat{x}_1-\ell}^{\widehat{x}_1+\ell} \sigma_{3i}(x_1, 0^{\pm})dx_1, \end{aligned} \tag{4}$$

where $\widehat{x}_1$ and $\ell$ are the midpoint and the half-length of the macroscopic portion.

The interfacial conditions in the macro-level spring model for the microscopically damaged interface are (see, for example, Fan and Sze [6] and Benveniste and Miloh [3])

$$\widehat{k}(\widehat{u}_3(\widehat{x}_1, 0^+) - \widehat{u}_3(\widehat{x}_1, 0^-)) = \widehat{\sigma}_{32}(\widehat{x}_1, 0^+) = \widehat{\sigma}_{32}(\widehat{x}_1, 0^-), \tag{5}$$

where $\widehat{k}$ is the effective stiffness of the interface. It is assumed here that the interface is homogeneously damaged at the macro level so that $\widehat{k}$ is a constant.

The problem of interest here is to investigate the effect of the plane boundary $x_2 = h$ of the thin layer on the effective stiffness $\widehat{k}$ of the interface.

# 3 Micromechanical analysis of the interface

As in Wang, Ang and Fan [11], the microscopically damaged interface is modeled as containing periodic arrays of interfacial micro-cracks. More specifically, $M$ arbitrarily located micro-cracks of possibly different lengths lie on the part of the interface where $0 < x_1 < L$, $x_2 = 0$. The tips of a typical $m$-th micro-crack on this part of the interface are given by $(a^{(m)}, 0)$ and $(b^{(m)}, 0)$, where $a^{(m)}$ and $b^{(m)}$ are constants such that $0 < a^{(1)} < b^{(1)} < a^{(2)} < b^{(2)} < \cdots < a^{(M)} < b^{(M)} < L$. On the remaining parts of the interface, the micro-cracks are given by $a^{(m)} + nL < x_1 < b^{(m)} + nL$ for $m = 1, 2, \cdots, M$ and $n = \pm 1, \pm 2, \cdots$, that is, the remaining micro-cracks are periodically distributed exact replicas of the $M$ micro-cracks on the interval $0 < x_1 < L$, $x_2 = 0$. Refer to Figure 1.

The fraction of the interface damaged by the micro-cracks is given by $\rho$ where

$$\rho = \frac{1}{L} \sum_{m=1}^{M} (b^{(m)} - a^{(m)}). \tag{6}$$

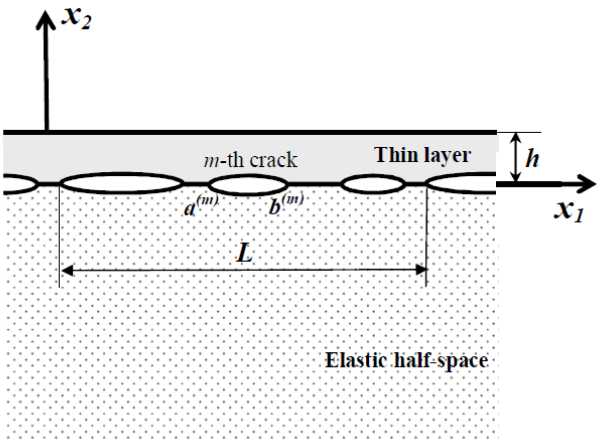


**Figure 1.** The micro-cracked interface between a thin layer and a half-space.

The bimaterial is acted upon by an external uniform antiplane shear stress load. The micro-cracks are assumed traction free. For micromechanical analysis of the micro-cracked interface, the governing partial differential equation (3) together with (2) is to be solved in the bimaterial subject to

$$\begin{array}{l} \sigma_{32}(x_1, 0^{\pm}) = 0 \text{ for } (x_1, 0^{\pm}) \text{ on the micro-cracks,} \\ \left.\begin{array}{l} u_3(x_1, 0^+) = u_3(x_1, 0^-) \\ \sigma_{32}(x_1, 0^+) = \sigma_{32}(x_1, 0^-) \end{array}\right\} \text{ for } (x_1, 0^{\pm}) \text{ outside the micro-cracks,} \end{array} \tag{7}$$

and

$$\begin{array}{l} \sigma_{32}(x_1, h) = S_0 \text{ for } x_1 \in (-\infty, \infty), \\ \sigma_{32}(x_1, x_2) \to S_0 \text{ as } x_2 \to -\infty, \end{array} \tag{8}$$

where $S_0$ is a given positive constant.

Two different micromechanical models are used here for estimating the effective stiffness $\widehat{k}$ of the micro-cracked interface described above. One is a three-phase model which simplifies a period length of the micro-cracked interface to a single micro-crack, perfectly bonded parts and an effective region. The other is a micromechanical-statistical model in which the positions and lengths of a sufficiently large number of micro-cracks lying on a period of the interface are chosen using statistical simulations.

## 3.1 Three-phase model

The three-phase model here models the portion of the micro-cracked interface on $0 < x_1 < L$ as comprising (i) a single representative micro-crack in the region $c^{(1)} < x_1 < d^{(1)}$, $x_2 = 0$, (ii) perfectly bonded parts in the regions $0 < x_1 < c^{(1)}$ and $d^{(1)} < x_1 < c^{(2)}$ on $x_2 = 0$, and (iii) an effective region $c^{(2)} < x_1 < d^{(2)}$, $x_2 = 0$, which describes the behaviors of the interface using the macro-level spring model. Note that $c^{(1)}$, $c^{(2)}$, $d^{(1)}$ and $d^{(2)}$ are constants such that $0 < c^{(1)} < d^{(1)} < c^{(2)} < d^{(2)} = L$, $c^{(1)} = c^{(2)} - d^{(1)}$ and $c^{(2)}$ is much smaller than $L$. The geometry of the entire interface in the three-phase model is periodic with period $L$. Refer to Figure 2.

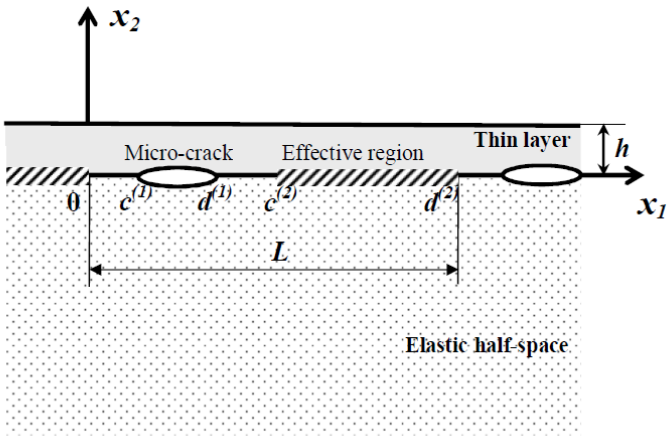


**Figure 2.** A sketch of the three-phase model

For the three-phase model, the damage ratio $\rho$ corresponding to (6) is given by

$$\rho = \frac{d^{(1)} - c^{(1)}}{c^{(2)}}. \tag{9}$$

The interfacial conditions for the three-phase model are

$$\begin{aligned} &\sigma_{32}(x_1, 0^{\pm}) = 0 \text{ for } (x_1, 0^{\pm}) \in I_{\text{damage}}, \\ &\left.\begin{array}{rcl} \Delta u_3(x_1) & = & 0 \\ \sigma_{32}(x_1, 0^{+}) & = & \sigma_{32}(x_1, 0^{-}) \end{array}\right\} \text{ for } (x_1, 0^{\pm}) \in I_{\text{perfect}}, \\ &\widehat{k}\Delta u_3(x_1) = \sigma_{32}(x_1, 0^{\pm}) \text{ for } (x_1, 0^{\pm}) \in I_{\text{effective}}, \end{aligned} \tag{10}$$

where $\Delta u_3(x_1) = u_3(x_1, 0^{+}) - u_3(x_1, 0^{-})$ and

$$\begin{aligned} I_{\text{damage}} &= \bigcup_{n=-\infty}^{\infty} (c^{(1)} + nL, d^{(1)} + nL), \\ I_{\text{perfect}} &= \bigcup_{n=-\infty}^{\infty} (nL, c^{(1)} + nL) \cup (d^{(1)} + nL, c^{(2)} + nL), \\ I_{\text{effective}} &= \bigcup_{n=-\infty}^{\infty} (c^{(2)} + nL, d^{(2)} + nL). \end{aligned} \tag{11}$$

Note that the conditions over $I_{\text{effective}}$ in (10) follow those given in (5) for the macro-model of the microscopically damaged interface. As the effective stiffness $\widehat{k}$ is an unknown constant to be determined, another equation is needed to complete the formulation of the interfacial conditions. The equation is given by

$$\frac{\widehat{k}}{c^{(2)}} \int_{c^{(1)}}^{d^{(1)}} \Delta u_3(x_1) dx_1 = S_0. \tag{12}$$

It is derived from the relation

$$\widehat{k} \times (\text{average value of } \Delta u_3(x_1) \text{ over } 0 < x_1 < c^{(2)}) \ = S_0. \tag{13}$$

For the analysis of the three-phase model, the partial differential equation (3) together with (2) is to be solved in the bimaterial in Figure 2 subject to (8), (10) and (12).

## 3.2 Micromechanical-statistical model

To simulate the micro-cracked interface statistically, the $M$ micro-cracks over a period length of the interface are generated randomly. The length of a micro-crack follows a chosen statistical distribution and each micro-crack is positioned randomly. For a more realistic simulation of the variation of the micro-crack length, the chi-square distribution of degree of freedom $k$, denoted by $\chi^2(k)$, is used to generate the lengths of $M$ micro-cracks. A $\chi^2$ distribution with a smaller degree of freedom has a probability density function skewed towards generating a greater number of shorter micro-cracks. As an example, the distribution of the micro-crack length generated by the $\chi^2(5)$ distribution is shown in Figure 3.

For fixed values of the damage ratio $\rho$ of the interface and the non-dimensionalized thin layer thickness $\widehat{h} = h/\widehat{a}$, where $\widehat{a}$ is the average half

crack length of the micro-cracks on the interface, the effective stiffness of the micro-cracked interface is estimated as follows. A random sample of $N$ interfaces is formed by choosing randomly $N$ sets of $M$ micro-cracks as described above. For the $n$-th interface, the governing partial differential equation (3) with (2) is solved in the bimaterial subject to the conditions in (7) and (8). Once the displacement jump $\Delta u_3(x_1)$ is known on the $M$ micro-cracks, the effective stiffness $\widehat{k}_n$ of the $n$-th interface may be obtained using

$$\widehat{k}_n = S_0 L[\sum_{m=1}^{M} \int_{a^{(m)}}^{b^{(m)}} \Delta u_3(x_1) dx_1]^{-1}. \tag{14}$$

The non-dimensionalized effective stiffness $\widehat{a}_n \widehat{k}_n / \sqrt{\lambda_{11}^{(2)} \lambda_{22}^{(2)} - (\lambda_{12}^{(2)})^2}$ is computed from (14).

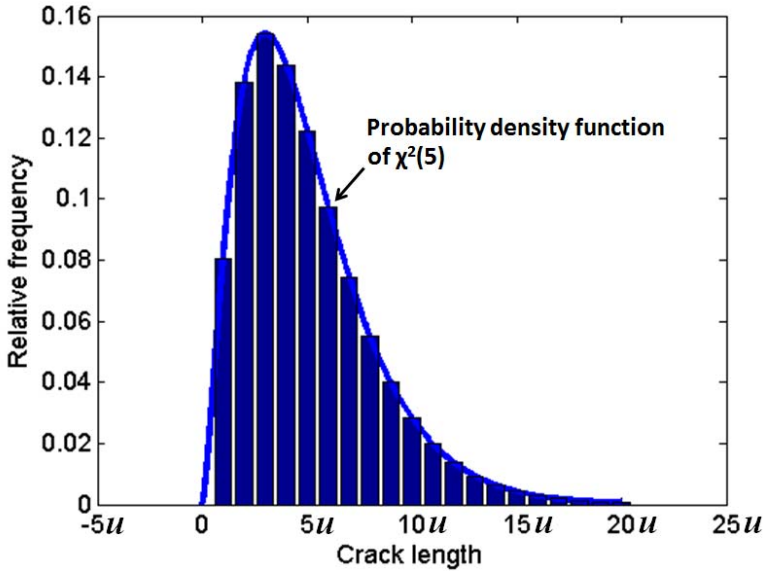


**Figure 3**. Distribution of the micro-cracks lengths generated by the $\chi^2(5)$ distribution. Note that $u$ denotes a unit length.

If the non-dimensionalized effective stiffness from the $N$ interfaces are given by $y_1, y_2, \cdots, y_{N-1}$ and $y_N$, the sample mean $\mu$ of the non-dimensionalized effective stiffness is given by

$$\mu = \frac{1}{N}\sum_{n=1}^{N} y_n, \tag{15}$$

and the standard deviation of the non-dimensionalized effective stiffness from the sample mean $\mu$ is

$$s = \sqrt{\frac{1}{N-1}\sum_{n=1}^{N}(y_n - \mu)^2}. \tag{16}$$

# 4 Hypersingular integral equations

In this section, the analysis in Wang, Ang and Fan [11] is extended to derive hypersingular integral equations for the boundary value problems of the three-phase and the micromechanical-statistical models. The unknown functions in the hypersingular integral equations are the interfacial displacement jump $\Delta u_3$ on the damaged parts of the interface and the displacement $u_3$ on the plane boundary $x_2 = h$.

## 4.1 Three-phase model

For the boundary value problem of the three-phase model, the boundary integral equation of (3) as given in Clements [5] may be used together with the perfect interface Green's function in Berger and Karageorghis [4] to derive

$$\begin{aligned} u_3(\xi_1,\xi_2) &= \frac{S_0\xi_2}{\lambda_{22}(\xi_1,\xi_2)} + \sum_{n=-\infty}^{\infty}\int_{nL}^{(n+1)L} u^*(x_1)\Lambda(x_1,h;\xi_1,\xi_2)dx_1 \\ &\quad - \sum_{n=-\infty}^{\infty}\sum_{m=1}^{2}\int_{c^{(m)}+nL}^{d^{(m)}+nL} \Delta u_3(x_1)\Lambda(x_1,0^+;\xi_1,\xi_2)dx_1 \\ \text{for } 0 &< \xi_2 < h, \end{aligned} \tag{17}$$

where $u^*(x_1) = u_3(x_1, h) - S_0 h/\lambda_{22}^{(1)}$ and

$$\Lambda(x_1, x_2; \xi_1, \xi_2) = \frac{1}{2\pi\beta^{(1)}} \mathrm{Re}\{\frac{L_2^{(1)}}{x_1 - \xi_1 + \tau^{(1)}(x_2 - \xi_2)}\}$$
$$+\frac{\beta^{(1)} - \beta^{(2)}}{2\pi\beta^{(1)}(\beta^{(1)} + \beta^{(2)})} \mathrm{Re}\{\frac{L_2^{(1)}}{x_1 - \xi_1 + \tau^{(1)} x_2 - \overline{\tau}^{(1)}\xi_2}\}, \tag{18}$$

where $\beta^{(p)} = \sqrt{\lambda_{11}^{(p)}\lambda_{22}^{(p)} - [\lambda_{12}^{(p)}]^2}$, $\tau^{(p)} = (-\lambda_{12}^{(p)} + i\beta^{(p)})/\lambda_{22}^{(p)}$, $L_2^{(p)} = \lambda_{11}^{(p)} + \tau^{(p)}\lambda_{12}^{(p)}$ and $i = \sqrt{-1}$. Note that the overhead bar over a complex number denotes the complex conjugate of the number.

The use of (1) and (17) gives

$$\begin{aligned}\sigma_{32}(\xi_1, \xi_2) &= S_0 + \sum_{n=-\infty}^{\infty} \int_{nL}^{(n+1)L} u^*(x_1)\Gamma(x_1, h; \xi_1, \xi_2) dx_1 \\ &\quad - \sum_{n=-\infty}^{\infty} \sum_{m=1}^{2} \int_{c^{(m)}+nL}^{d^{(m)}+nL} \Delta u_3(x_1)\Gamma(x_1, 0^+; \xi_1, \xi_2) dx_1 \\ &\quad \text{for } 0 < \xi_2 < h, \end{aligned} \tag{19}$$

where

$$\Gamma(x_1, x_2; \xi_1, \xi_2) = \frac{1}{2\pi\beta^{(1)}} \mathrm{Re}\{\frac{(L_2^{(1)})^2}{[x_1 - \xi_1 + \tau^{(1)}(x_2 - \xi_2)]^2}\}$$
$$+\frac{\beta^{(1)} - \beta^{(2)}}{2\pi\beta^{(1)}(\beta^{(1)} + \beta^{(2)})} \mathrm{Re}\{\frac{L_2^{(1)}\overline{L}_2^{(1)}}{[x_1 - \xi_1 + \tau^{(1)} x_2 - \overline{\tau}^{(1)}\xi_2]^2}\}. \tag{20}$$

Note that the conditions on $I_{\mathrm{perfect}}$ in (10) and the far-field condition in the second line of (8) are satisfied by (18) and (19).

From the fact that $u^*(x_1) = u_3(x_1, h) - S_0 h/\lambda_{22}^{(1)}$ and $\Delta u_3(x_1)$ are periodic functions of $x_1$ with period $L$, (19) and the formula (Wang, Ang and Fan

[11])

$$\sum_{n=1}^{\infty} \frac{1}{(a \pm bn)^2} = \frac{1}{b^2}\psi_1(1 \pm \frac{a}{b}) \text{ for } \mathrm{Re}\{1 \pm \frac{a}{b}\} > 0, \tag{21}$$

where $\psi_1$ is the trigamma function, the boundary condition on the plane boundary $x_2 = h$ as given in (8) gives rise to the hypersingular integral equations

$$\begin{aligned} & \oint_0^{d^{(2)}} \frac{u^*(x_1)}{(x_1-\xi_1)^2} dx_1 \\ & + \int_0^{d^{(2)}} u^*(x_1)[\Theta(x_1,\xi_1) - \frac{\beta^{(1)}-\beta^{(2)}}{\beta^{(1)}+\beta^{(2)}}\Omega(x_1,-\xi_1,\frac{2\beta^{(1)}}{\lambda_{22}^{(1)}}h)]dx_1 \\ & -\frac{2\beta^{(2)}}{\beta^{(1)}+\beta^{(2)}}\sum_{k=1}^{2}\int_{c^{(k)}}^{d^{(k)}} \Delta u_3(x_1)\Omega(x_1,-\xi_1+\frac{\lambda_{21}^{(1)}}{\lambda_{22}^{(1)}}h,-\frac{\beta^{(1)}}{\lambda_{22}^{(1)}}h)dx_1 \\ = \;& 0 \;\text{ for } 0 < \xi_1 < d^{(2)}, \end{aligned} \tag{22}$$

and the conditions in (10) for $I_{\text{damage}}$ and $I_{\text{effective}}$ yield

$$\begin{aligned} & \int_0^{d^{(2)}} u^*(x_1)\Omega(x_1,-\xi_1-\frac{\lambda_{21}^{(1)}}{\lambda_{22}^{(1)}}h,\frac{\beta^{(1)}}{\lambda_{22}^{(1)}}h)dx_1 \\ & -\oint_{c^{(n)}}^{d^{(n)}} \frac{\Delta u_3(x_1)}{(x_1-\xi_1)^2}dx_1 - \sum_{\substack{k=1\\k\neq n}}^{2}\int_{c^{(k)}}^{d^{(k)}} \frac{\Delta u_3(x_1)}{(x_1-\xi_1)^2}dx_1 \\ & -\sum_{k=1}^{2}\int_{c^{(k)}}^{d^{(k)}} \Delta u_3(x_1)\Theta(x_1,\xi_1)dx_1 \\ = \;& \frac{\pi(\beta^{(1)}+\beta^{(2)})(S_0-\delta^{(n2)}\widehat{k}\Delta u_3(\xi_1))}{\beta^{(1)}\beta^{(2)}} \text{ for } c^{(n)} < \xi_1 < d^{(n)} \; (n=1,2), \end{aligned} \tag{23}$$

where $\oint$ denotes that the integral is to be interpreted in the Hadamard finite-part sense, $\delta^{(mn)}$ is such that $\delta^{(mn)} = 1$ if $m = n$ and $\delta^{(mn)} = 0$ if

$m \neq n$, and $\Theta(x_1, \xi_1)$ and $\Omega(x_1, \xi_1, \xi_2)$ are defined by

$$\begin{aligned}
\Theta(x_1, \xi_1) &= \frac{1}{L^2}\psi_1(\frac{L + x_1 - \xi_1}{L}) + \frac{1}{L^2}\psi_1(\frac{L + \xi_1 - x_1}{L}), \\
\Omega(x_1, \xi_1, \xi_2) &= \frac{(x_1 + \xi_1)^2 - {\xi_2}^2}{((x_1 + \xi_1)^2 + \xi_2^2)^2} + \frac{1}{2L^2}\psi_1(\frac{L + \xi_1 + x_1 - \xi_2 i}{L}) \\
&\quad + \frac{1}{2L^2}\psi_1(\frac{L + \xi_1 + x_1 + \xi_2 i}{L}) + \frac{1}{2L^2}\psi_1(\frac{-L + \xi_1 + x_1 - \xi_2 i}{-L}) \\
&\quad + \frac{1}{2L^2}\psi_1(\frac{-L + \xi_1 + x_1 + \xi_2 i}{-L}). \qquad (24)
\end{aligned}$$

In the three-phase model, the hypersingular integral equations in (23) and (24) are to be solved together with (12) for the unknown functions $u^*$ and $\Delta u_3$ and the effective stiffness $\widehat{k}$.

## 4.2 Micromechanical-statistical model

The boundary value problem for the micromechanical statistical model requires solving (3) with (2) in the bimaterial subject to the conditions in (7) and (8). As in the analysis for the three-phase model, the boundary integral equation of (3) together with the perfect interface Green's function may be used to derive

$$\begin{aligned}
u_3(\xi_1, \xi_2) &= \frac{S_0 \xi_2}{\lambda_{22}(\xi_1, \xi_2)} + \sum_{n=-\infty}^{\infty} \int_{nL}^{(n+1)L} u^*(x_1) \Lambda(x_1, h; \xi_1, \xi_2) dx_1 \\
&\quad - \sum_{n=-\infty}^{\infty} \sum_{m=1}^{M} \int_{a^{(m)}+nL}^{b^{(m)}+nL} \Delta u_3(x_1) \Lambda(x_1, 0^+; \xi_1, \xi_2) dx_1 \\
&\qquad \text{for } 0 < \xi_2 < h. \qquad (25)
\end{aligned}$$

and

$$\begin{aligned}\sigma_{32}(\xi_1,\xi_2) &= S_0+\sum_{n=-\infty}^{\infty}\int_{nL}^{(n+1)L} u^*(x_1)\Gamma(x_1,h;\xi_1,\xi_2)dx_1 \\ &\quad -\sum_{n=-\infty}^{\infty}\sum_{m=1}^{M}\int_{a^{(m)}+nL}^{b^{(m)}+nL}\Delta u_3(x_1)\Gamma(x_1,0^+;\xi_1,\xi_2)]dx_1 \\ &\qquad\qquad \text{for } 0<\xi_2<h. \end{aligned} \tag{26}$$

From (26), the conditions on the plane boundary $x_2 = h$ (in (8)) and on the micro-cracks (in (7)) may be rewritten respectively in terms of the hypersingular integral equations

$$\begin{aligned}&\oint_0^L \frac{u^*(x_1)}{(x_1-\xi_1)^2}dx_1 \\ &+\int_0^L u^*(x_1)[\Theta(x_1,\xi_1)-\frac{\beta^{(1)}-\beta^{(2)}}{\beta^{(1)}+\beta^{(2)}}\Omega(x_1,-\xi_1,\frac{2\beta^{(1)}}{\lambda_{22}^{(1)}}h)]dx_1 \\ &-\frac{2\beta^{(2)}}{\beta^{(1)}+\beta^{(2)}}\sum_{m=1}^{M}\int_{a^{(m)}}^{b^{(m)}}\Delta u_3(x_1)\Omega(x_1,-\xi_1+\frac{\lambda_{21}^{(1)}}{\lambda_{22}^{(1)}}h,-\frac{\beta^{(1)}}{\lambda_{22}^{(1)}}h)dx_1 \\ =\;& 0 \text{ for } 0<\xi_1<L\ , \end{aligned} \tag{27}$$

and

$$\begin{aligned}&\int_0^L u^*(x_1)\Omega(x_1,-\xi_1-\frac{\lambda_{21}^{(1)}}{\lambda_{22}^{(1)}}h,\frac{\beta^{(1)}}{\lambda_{22}^{(1)}}h)dx_1 \\ &-\oint_{a^{(n)}}^{b^{(n)}}\frac{\Delta u_3(x_1)}{(x_1-\xi_1)^2}dx_1-\sum_{\substack{m=1\\m\neq n}}^{M}\int_{a^{(m)}}^{b^{(m)}}\frac{\Delta u_3(x_1)}{(x_1-\xi_1)^2}dx_1 \\ &-\sum_{m=1}^{M}\int_{a^{(m)}}^{b^{(m)}}\Delta u_3(x_1)\Theta(x_1,\xi_1)dx_1 \\ =\;& S_0\frac{\pi(\beta^{(1)}+\beta^{(2)})}{\beta^{(1)}\beta^{(2)}},\ \text{for } a^{(n)}<\xi_1<b^{(n)}\ (n=1,2,\cdots,M). \end{aligned} \tag{28}$$

For statistically generated micro-cracks over a period length of the interface $x_2 = 0$, the hypersingular integral equations in (27) and (28) are to

be solved for the unknown functions $u^*$ and $\Delta u_3$ to calculate the effective stiffness in (14).

# 5 Numerical procedures

Numerical procedures for solving the hypersingular integral equations of the three-phase and the micromechanical-statistical models are outlined here. The boundary value problem for each of the models is eventually reduced to solving a system of linear algebraic equations.

For treating the integrals involving the unknown function $u^*(x_1)$ on the exterior boundary of the thin layer in both models, the interval $0 \leq x_1 \leq d^{(2)}$ is divided up into $N_{\rm t}$ equal subintervals. The $j$-th subinterval is given by $x_{\rm t}^{(j)} \leq x_1 \leq y_{\rm t}^{(j)}$. Over each of the subintervals, $u^*$ is approximated as a constant, that is,

$$\frac{\beta^{(2)}}{S_0} u^*(x_1) \simeq v^{(j)} \text{ (constant) for } x_{\rm t}^{(j)} \leq x_1 \leq y_{\rm t}^{(j)}, \tag{29}$$

where $v^{(1)}$, $v^{(2)}$, $\cdots$, $v^{(N_{\rm t}-1)}$ and $v^{(N_{\rm t})}$ are constants to be determined.

## 5.1 Three-phase model

The three-phase model requires approximating the displacement jump $\Delta u_3(x_1)$ over the intervals $c^{(1)} \leq x_1 \leq d^{(1)}$ ("the micro-crack") and $c^{(2)} \leq x_1 \leq d^{(2)}$ ("the effective region").

The displacement jump $\Delta u_3(x_1)$ over $c^{(1)} \leq x_1 \leq d^{(1)}$ shows a strong variation behaving like $\sqrt{(x_1 - c^{(1)})(d^{(1)} - x_1)}$ near $x_1 = c^{(1)}$ and $x_1 = d^{(1)}$.

It is approximated as in Kaya and Erdogan [7] by using

$$\begin{aligned}\frac{\beta^{(2)}}{S_0}\Delta u_3(x_1) \;&\simeq\; \sqrt{(x_1-c^{(1)})(d^{(1)}-x_1)}\\ &\quad\times\sum_{m=1}^{N_c}\alpha^{(m)}U^{(m-1)}\Big(\frac{2x_1-c^{(1)}-d^{(1)}}{d^{(1)}-c^{(1)}}\Big)\\ &\qquad\text{for } c^{(1)}\le x_1\le d^{(1)},\end{aligned}\tag{30}$$

where $N_c$ is a positive integer, $\alpha^{(1)}$, $a^{(2)}$, $\cdots$, $\alpha^{(N_c-1)}$ and $\alpha^{(N_c)}$ are constant coefficients to be determined and $U^{(m)}(x)$ is the $m$-th order Chebyshev polynomials of the second kind. Note that $N_c$ may be required to be sufficiently large for (30) to be a good approximation. Details on such an approximation may also be found in Ang [2].

For approximating $\Delta u_3(x_1)$ over the effective region, the interval $c^{(2)} \le x_1 \le d^{(2)}$ is divided into $N_e$ subintervals. The $j$-th subinterval is given by $x_e^{(j)} \le x_1 \le y_e^{(j)}$. More specifically, $x_e^{(j)}$ and $y_e^{(j)}$ are given by

$$\left.\begin{aligned}x_e^{(j)} &= \frac{c^{(2)}+d^{(2)}}{2}-\frac{d^{(2)}-c^{(2)}}{2}\cos\Big(\frac{[j-1]\pi}{N_e}\Big)\\ y_e^{(j)} &= \frac{c^{(2)}+d^{(2)}}{2}-\frac{d^{(2)}-c^{(2)}}{2}\cos\Big(\frac{j\pi}{N_e}\Big)\end{aligned}\right\}\ \text{for } j=1,2,\cdots,N_e.\tag{31}$$

The displacement jump $\Delta u_3(x_1)$ is approximated as a constant over each of the subintervals, that is,

$$\frac{\beta^{(1)}}{S_0}\Delta u_3(x_1)\simeq w^{(m)}\ \text{(constant) for for } x_e^{(j)}\le x_1\le y_e^{(j)},\tag{32}$$

where $w^{(1)}$, $w^{(2)}$, $\cdots$, $w^{(N_e-1)}$ and $w^{(N_e)}$ are constants to be determined.

With the approximations above, if $\xi_1$ in (22) is taken in turn to be given by $\widehat{x}_t^{(n)} = (x_t^{(n)}+y_t^{(n)})/2$ for $n=1,2,...,N_t$, the hypersingular integral equations

may be reduced to the linear algebraic equations

$$\begin{aligned}
&\sum_{j=1}^{N_{\rm t}} v^{(j)}\{-\frac{1}{(y_{\rm t}^{(j)}-\widehat{x}_{\rm t}^{(n)})}+\frac{1}{(x_{\rm t}^{(j)}-\widehat{x}_{\rm t}^{(n)})}\\
&+\int_{x_{\rm t}^{(j)}}^{y_{\rm t}^{(j)}}[\Theta(x_1,\xi_1)-\frac{\beta^{(1)}/\beta^{(2)}-1}{\beta^{(1)}/\beta^{(2)}+1}\Omega(x_1,-\widehat{x}_{\rm t}^{(n)},\frac{2\beta^{(1)}}{\lambda_{22}^{(1)}}h)]dx_1\}\\
&-\frac{2}{\beta^{(1)}/\beta^{(2)}+1}\sum_{m=1}^{N_{\rm c}}\alpha^{(m)}\int_{c^{(1)}}^{d^{(1)}}\sqrt{(x_1-c^{(1)})(d^{(1)}-x_1)}\\
&\times U^{(m-1)}(\frac{2x_1-d^{(1)}-c^{(1)}}{d^{(1)}-c^{(1)}})\Omega(x_1,-\widehat{x}_{\rm t}^{(n)}+\frac{\lambda_{21}^{(1)}}{\lambda_{22}^{(1)}}h,-\frac{\beta^{(1)}}{\lambda_{22}^{(1)}}h)dx_1\\
&-\frac{2}{\beta^{(1)}/\beta^{(2)}+1}\sum_{j=1}^{N_{\rm e}}w^{(j)}\int_{x_{\rm e}^{(j)}}^{y_{\rm e}^{(j)}}\Omega(x_1,-\widehat{x}_{\rm t}^{(n)}+\frac{\lambda_{21}^{(1)}}{\lambda_{22}^{(1)}}h,-\frac{\beta^{(1)}}{\lambda_{22}^{(1)}}h)dx_1\\
=\;& 0 \text{ for } n=1,2,...,N_{\rm t}.
\end{aligned} \tag{33}$$

If $\xi_1$ in (23) for $c^{(1)}<\xi_1<d^{(1)}$ (over the micro-crack) is taken in turn by

$$\begin{aligned}
\xi_1 \;=\; \xi^{(p)} &\equiv \frac{1}{2}(c^{(1)}+d^{(1)})+\frac{1}{2}(d^{(1)}-c^{(1)})\cos(\frac{[2p-1]\pi}{2N_{\rm c}})\\
&\text{for } p=1,2,...,N_{\rm c},
\end{aligned} \tag{34}$$

the hypersingular singular equations may be approximately reduced to the

linear algebraic equations

$$
\begin{aligned}
&\sum_{j=1}^{N_{\rm t}} v^{(j)} \int_{x_{\rm t}^{(j)}}^{y_{\rm t}^{(j)}} \Omega(x_1, -\xi^{(p)} - \frac{\lambda_{21}^{(1)}}{\lambda_{22}^{(1)}} h, \frac{\beta^{(1)}}{\lambda_{22}^{(1)}} h) dx_1 \\
&+\pi \sum_{m=1}^{N_{\rm c}} \alpha^{(m)} m U^{(m-1)}(\frac{2\xi^{(p)} - d^{(1)} - c^{(1)}}{d^{(1)} - c^{(1)}}) \\
&-\sum_{m=1}^{N_{\rm c}} \alpha^{(m)} \int_{c^{(1)}}^{d^{(1)}} \sqrt{(x_1 - c^{(1)})(d^{(1)} - x_1)} \\
&\times U^{(m-1)}(\frac{2x_1 - d^{(1)} - c^{(1)}}{d^{(1)} - c^{(1)}}) \Theta(x_1, \xi^{(p)}) dx_1 \\
&-\sum_{j=1}^{N_{\rm e}} w^{(j)} \left\{ -\frac{1}{y_{\rm e}^{(j)} - \xi^{(p)}} + \frac{1}{x_{\rm e}^{(j)} - \xi^{(p)}} + \int_{x_{\rm e}^{(j)}}^{y_{\rm e}^{(j)}} \Theta(x_1, \xi^{(p)}) dx_1 \right\} \\
= \quad & (\frac{\beta^{(2)}}{\beta^{(1)}} + 1)\pi, \ \text{for } p = 1, 2, ..., N_{\rm c},
\end{aligned}
\tag{35}
$$

If $\xi_1$ in (23) for $c^{(2)} < \xi_1 < d^{(2)}$ (over the effective region) is taken to be given by the midpoint of each of the elements on the effective region, that is, $\xi_1 \equiv \widehat{x}_{\rm e}^{(n)} = (x_{\rm e}^{(n)} + y_{\rm e}^{(n)})/2$, the hypersingular integral equations approximately give rise to

$$
\begin{aligned}
&\sum_{j=1}^{N_{\rm t}} v^{(j)} \int_{x_{\rm t}^{(j)}}^{y_{\rm t}^{(j)}} \Omega(x_1, -\widehat{x}_{\rm e}^{(n)} - \frac{\lambda_{21}^{(1)}}{\lambda_{22}^{(1)}}h, \frac{\beta^{(1)}}{\lambda_{22}^{(1)}}h)dx_1 \\
&-\sum_{m=1}^{N_{\rm c}} \alpha^{(m)} \int_{c^{(1)}}^{d^{(1)}} \sqrt{(x_1 - c^{(1)})(d^{(1)} - x_1)} \\
&\times U^{(m-1)}(\frac{2x_1 - d^{(1)} - c^{(1)}}{d^{(1)} - c^{(1)}})[\frac{1}{(x_1 - \widehat{x}_{\rm e}^{(n)})^2} + \Theta(x_1, \widehat{x}_{\rm e}^{(n)})]dx_1 \\
&-\sum_{i=1}^{N_{\rm e}} w^{(i)} \left\{ -\frac{1}{y_{\rm e}^{(i)} - \widehat{x}_{\rm e}^{(n)}} + \frac{1}{x_{\rm e}^{(i)} - \widehat{x}_{\rm e}^{(n)}} \right. \\
&\left. + \int_{x_{\rm e}^{(i)}}^{y_{\rm e}^{(i)}} \Theta(x_1, \widehat{x}_{\rm e}^{(n)})dx_1 - (\frac{\beta^{(2)}}{\beta^{(1)}} + 1)\frac{\widehat{k}}{\beta^{(2)}}\pi\delta^{(in)} \right\} \\
= \;& (\frac{\beta^{(2)}}{\beta^{(1)}} + 1)\pi, \text{ for } n = 1, 2, ..., N_{\rm e}.
\end{aligned}
\tag{36}
$$

Use of (30) in (12) gives

$$
\begin{aligned}
\frac{1}{\beta^{(2)}}\widehat{k} \;=\; & c^{(2)}[\sum_{m=1}^{N_{\rm c}} \alpha^{(m)} \int_{c^{(1)}}^{d^{(1)}} \sqrt{(x_1 - c^{(1)})(d^{(1)} - x_1)} \\
& \times U^{(m-1)}(\frac{2x_1 - d^{(1)} - c^{(1)}}{d^{(1)} - c^{(1)}})dx_1]^{-1}.
\end{aligned}
\tag{37}
$$

The equations in (33), (35), (36) and (37) may be solved simultaneously for the unknowns $v^{(j)}$ $(j = 1, 2, ..., N_{\rm t})$, $\alpha^{(m)}$ $(m = 1, 2, ..., N_{\rm c})$, $w^{(j)}$ $(j = 1, 2, ..., N_{\rm e})$ and $\widehat{k}$. An iterative method may be used to solve the equations as follows. With a guessed value of $\widehat{k}$, (33), (35) and (36) are solved as a system of $N_{\rm t} + N_{\rm e} + N_{\rm c}$ linear algebraic equations for $v^{(j)}$ $(j = 1, 2, ..., N_{\rm t})$, $\alpha^{(m)}$ $(m = 1, 2, ..., N_{\rm c})$ and $w^{(j)}$ $(j = 1, 2, ..., N_{\rm e})$. The value of $\widehat{k}$ is then updated using (37). With the updated value of $\widehat{k}$, (33), (35) and (36) are

solved again. The procedure is repeated until $\widehat{k}$ is observed to converge to a prescribed number of significant figures.

Note that all the integrals in (33), (35), (36) and (37) may be evaluated accurately by using suitable integration quadratures. Specifically, the integrals containing the term $\sqrt{(x_1 - c^{(1)})(d^{(1)} - x_1)}$ in the integrands may be computed with good accuracy by using formula (25.4.40) in Abramowitz and Stegun [1] and the other integrals by the Simpson's rule.

## 5.2 Micromechanical-statistical model

For the micro-cracks in the micromechanical-statistical model, the displacement jump $\Delta u_3(x_1)$ is approximated using

$$\begin{aligned} \frac{\beta^{(2)}}{S_0}\Delta u_3(x_1) &\simeq \sqrt{(x_1 - a^{(k)})(b^{(k)} - x_1)} \\ &\quad \times \sum_{m=1}^{N_c^{(k)}} \alpha^{(km)} U^{(m-1)}\left(\frac{2x_1 - b^{(k)} - a^{(k)}}{b^{(k)} - a^{(k)}}\right) \\ \text{for } a^{(k)} &< x_1 < b^{(k)},\ k = 1, 2, ..., M, \end{aligned} \tag{38}$$

where $\alpha^{(km)}$ are unknowns to be determined.

With the above approximations, if $\xi_1$ in (19) is taken in turn to be given by $\widehat{x}_{\rm t}^{(n)}$ for $n = 1, 2, ..., N_{\rm t}$, the hypersingular integral equations may be approximately reduced to linear algebraic equations

$$\sum_{j=1}^{N_t} v^{(j)} \left\{ -\frac{1}{y_t^{(j)} - \widehat{x}_t^{(n)}} + \frac{1}{x_t^{(j)} - \widehat{x}_t^{(n)}} \right.$$
$$\left. + \int_{x_t^{(j)}}^{y_t^{(j)}} [\Theta(x_1, \widehat{x}_t^{(n)}) - \frac{\beta^{(1)}/\beta^{(2)} - 1}{\beta^{(1)}/\beta^{(2)} + 1} \Omega(x_1, -\widehat{x}_t^{(n)}, \frac{2\beta^{(1)}}{\lambda_{22}^{(1)}} h)] dx_1 \right\}$$
$$- \frac{2}{\beta^{(1)}/\beta^{(2)} + 1} \sum_{k=1}^{M} \sum_{m=1}^{N_c^{(k)}} \alpha^{(km)} \int_{a^{(k)}}^{b^{(k)}} \sqrt{(x_1 - a^{(k)})(b^{(k)} - x_1)}$$
$$\times U^{(m-1)}(\frac{2x_1 - b^{(k)} - a^{(k)}}{b^{(k)} - a^{(k)}}) \Omega(x_1, -\widehat{x}_t^{(n)} + \frac{\lambda_{21}^{(1)}}{\lambda_{22}^{(1)}} h, -\frac{\beta^{(1)}}{\lambda_{22}^{(1)}} h) dx_1$$
$$= \quad 0 \text{ for } n = 1, 2, ..., N_t. \tag{39}$$

Similarly, if $\xi_1$ in (20) is given in turn by

$$\xi_1 \quad = \quad \xi^{(kp)} \equiv \frac{1}{2}(a^{(k)} + b^{(k)}) + \frac{1}{2}(b^{(k)} - a^{(k)}) \cos(\frac{[2p-1]\pi}{2N_c^{(k)}})$$
$$\text{for } p = 1, 2, ..., N_c^{(k)} \ (k = 1, 2, ..., M), \tag{40}$$

the hypersingular integral equations may be approximately reduced to the linear algebraic equations

$$
\begin{aligned}
&\sum_{j=1}^{N_t} v^{(j)} \int_{x_t^{(j)}}^{y_t^{(j)}} \Omega(x_1, -\xi^{(np)} - \frac{\lambda_{21}^{(1)}}{\lambda_{22}^{(1)}}h, \frac{\beta^{(1)}}{\lambda_{22}^{(1)}}h)dx_1 \\
&+\pi \sum_{m=1}^{N_c^{(n)}} \alpha^{(nm)} m U^{(m-1)}(\frac{2\xi^{(np)} - b^{(n)} - a^{(n)}}{b^{(n)} - a^{(n)}}) \\
&-\sum_{\substack{k=1 \\ k\neq n}}^{M} \sum_{m=1}^{N_c^{(k)}} \alpha^{(km)} \int_{a^{(k)}}^{b^{(k)}} \frac{\sqrt{(x_1 - a^{(k)})(b^{(k)} - x_1)}}{(x_1 - \xi^{(np)})^2} \\
&\times U^{(m-1)}(\frac{2x_1 - b^{(k)} - a^{(k)}}{b^{(k)} - a^{(k)}})dx_1 \\
&-\sum_{k=1}^{M} \sum_{m=1}^{N_c^{(k)}} \alpha^{(km)} \int_{a^{(k)}}^{b^{(k)}} \sqrt{(x_1 - a^{(k)})(b^{(k)} - x_1)} \\
&\times U^{(m-1)}(\frac{2x_1 - b^{(k)} - a^{(k)}}{b^{(k)} - a^{(k)}})\Theta(x_1, \xi^{(np)})dx_1 \\
= \quad &(\frac{\beta^{(2)}}{\beta^{(1)}} + 1)\pi, \text{ for } p = 1, 2, ..., N_c^{(n)} \ (n = 1, 2, ..., M).
\end{aligned}
\tag{41}
$$

The linear algebraic equations (39) and (41) are solved simultaneously for the unknowns $v^{(j)}$ $(j = 1, 2, ..., N_{\rm t})$ and $\alpha^{(nm)}$ $(m = 1, 2, ..., N_c^{(n)};\ n = 1, 2, ..., M)$. From (14), the effective stiffness $\widehat{k}$ may be approximated as

$$
\begin{aligned}
\frac{1}{\beta^{(2)}}\widehat{k} \quad = \quad &L[\sum_{k=1}^{M} \sum_{m=1}^{N_c^{(k)}} \alpha^{(km)} \int_{a^{(k)}}^{b^{(k)}} \sqrt{(x_1 - a^{(k)})(b^{(k)} - x_1)} \\
&\times U^{(m-1)}(\frac{2x_1 - b^{(k)} - a^{(k)}}{b^{(k)} - a^{(k)}})dx_1]^{-1}.
\end{aligned}
\tag{42}
$$

# 6 Numerical checking

If the $M$ micro-cracks over the portion $0 < x_1 < L$, $x_2 = 0$, of the interface, as described at the beginning of Section 3, are taken to be of equal length and are evenly distributed on the interface, then the effective stiffness calculated by the numerical procedure for the micromechanical-statistical model in Subsection 5.2 should agree very closely with that given by the three-phase model in Subsection 5.1 (for the same corresponding input parameters).

To check numerically the observation above as well as to find out whether the three-phase model gives intuitively expected results or not, the numerical procedures in Subsections 5.1 and 5.2 are carried out using elastic modulus for isotropic materials as given by $\lambda_{ij}^{(n)} = \delta_{ij} G^{(n)}$,where $G^{(1)}$ and $G^{(2)}$ are the shear modulus of the thin layer and the half space respectively. For such materials, $\beta^{(n)} = G^{(n)}$ and the effective stiffness $\widehat{k}$ is such that $\widehat{k}/G^{(2)}$ is a function of $G^{(1)}/G^{(2)}$.

For the three-phase model in Subsection 5.1, the input parameters are taken to be given by $c^{(1)} = b - a$, $d^{(1)} = b + a$, $c^{(2)} = 2b$ and $d^{(2)} = L$, where $a$ and $b$ are positive numbers selected to be much smaller than $L$. Thus, the length of the representative micro-crack is $2a$ and the damage ratio $\rho$ is given by $a/b$. The thickness of the thin layer $h$ is non-dimensionalized as $\widehat{h} = h/a$. For selected $G^{(1)}/G^{(2)}$, $\widehat{h}$ and $\rho$, (33), (35) and (36) are solved with iterative procedure to estimate the non-dimensionalized effective stiffness $a\widehat{k}/G^{(2)}$ using (37). Note that $a\widehat{k}/G^{(2)}$ is independent of $a$.

For the numerical procedure in Subsection 5.2, the $M$ micro-cracks, each of length $2a$, are taken to be evenly distributed over the region $0 \leq x_1 \leq L$. For the numerical checking here, we take $M = 10$. For selected $G^{(1)}/G^{(2)}$, $\widehat{h}$ and $\rho$, (39) and (41) are solved to estimate $a\widehat{k}/G^{(2)}$ by using (42).

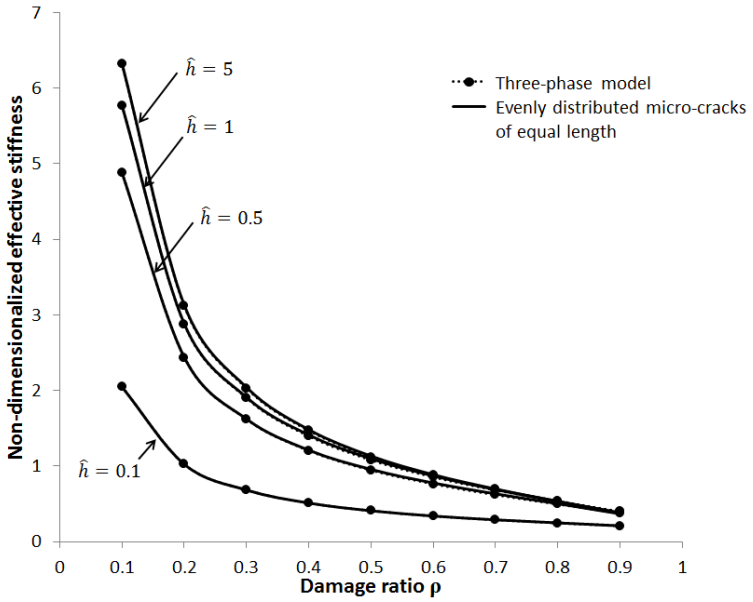


**Figure 4.** Plots of $a\widehat{k}/G^{(2)}$ against $\rho$ for the shear modulus ratio $G^{(1)}/G^{(2)} = 1$ and selected values of the thin layer thickness $\widehat{h}$.

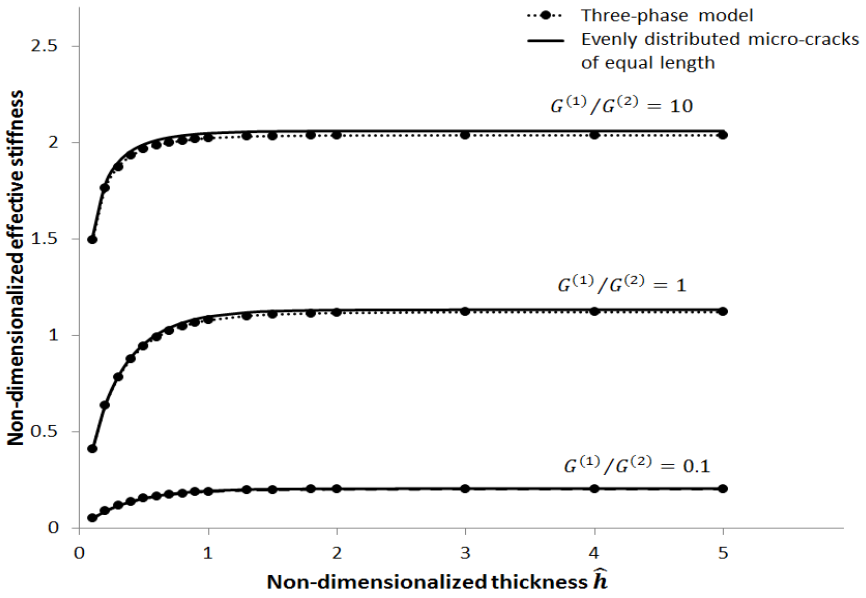


**Figure 5.** Plots of $a\widehat{k}/G^{(2)}$ against $\widehat{h}$ for the damage ratio $\rho = 0.5$ and selected values of the shear modulus ratio $G^{(1)}/G^{(2)}$.

Figure 4 plots the non-dimensionalized effective stiffness $a\widehat{k}/G^{(2)}$ against the damage ratio $\rho$ for selected $\widehat{h}$ and $G^{(1)}/G^{(2)} = 1$. As expected, the plots obtained by the numerical procedure in Subsection 5.1 are close to those calculated by the procedure for the three-phase model in Subsection 5.2. Further investigations using other values of $G^{(1)}/G^{(2)}$ show a very small difference between the effective stiffness calculated by the two numerical procedures. For fixed values of the non-dimensionalized thin layer thickness and the shear modulus ratio $G^{(1)}/G^{(2)}$, the percentage difference of the effective stiffness between the two models in Subsection 5.1 and 5.2 tends to become larger as $\rho$ increases. For $0.1 \leq \rho \leq 0.8$, the value of percentage difference between the two sets of numerical values of $a\widehat{k}/G^{(2)}$ is less than 3.5%, while for $\rho = 0.9$ the value of percentage difference is less than 4.9%.

For a fixed $\rho$, Figure 4 shows that $a\widehat{k}/G^{(2)}$ becomes larger with increasing thin layer thickness $\widehat{h}$. This is expected, as the interaction between the plane boundary and the interface becomes weaker and gives rise to smaller displacement jumps over the micro-cracks when the thickness $\widehat{h}$ is relatively small.

More results are given in Figure 5, where the damage ratio is fixed as $\rho = 0.5$ and $a\widehat{k}/G^{(2)}$ is plotted against the thin layer thickness $\widehat{h}$ for various selected values of $G^{(1)}/G^{(2)}$. It is observed that each of the plots for the non-dimensionalized effective stiffness tends to a constant value as $\widehat{h}$ increases. That constant value is very close to the corresponding values of the the non-dimensionalized effective stiffness computed using the models in Wang, Ang and Fan [11] for a microscopically damaged interface between two dissimilar half spaces. For a fixed $\widehat{h}$, Figure 5 also shows that the non-dimensionalized effective stiffness appears to be smaller for a smaller shear modulus ratio $G^{(1)}/G^{(2)}$. This suggests that the damaged interface is "strengthened" and has a greater effective stiffness when the shear modulus $G^{(1)}$ of the thin layer increases relative to the shear modulus $G^{(2)}$ of the half space. Lastly, as may be expected, the effective stiffness is observed to decrease as the damage ratio $\rho$ of the interface increases.

# 7 Micromechanical-statistical simulations

The micromechanical-statistical model is employed here to examine the effective stiffness of the micro-cracked interface for the case in which the materials occupying the thin layer and the elastic half space are isotropic with shear modulus $G^{(1)}$ and $G^{(2)}$ respectively. For the statistical simulation, an interface is formed by placing randomly $M$ micro-cracks with randomly generated lengths on a period length of the interface. The micro-crack length follows a

chosen $\chi^2$ distribution. For given shear modulus ratio $G^{(1)}/G^{(2)}$, damage ratio $\rho$ and non-dimensionalized thickness $\widehat{h} = h/\widehat{a}$ ($\widehat{a}$ is the average half length of the micro-cracks), the non-dimensionalized effective stiffness $\widehat{a}\widehat{k}/G^{(2)}$ is given by the mean of the non-dimensionalized effective stiffness of the $N$ randomly generated interfaces − the calculation of the mean is outlined in Subsection 3.2.

## 7.1 Influence of the micro-crack length distribution

The influence that the $\chi^2$ distribution used in generating the lengths of the micro-cracks has on $\widehat{a}\widehat{k}/G^{(2)}$ is examined here. For fixed $G^{(1)}/G^{(2)}$, $\rho$ and $\widehat{h}$, a sample of 50 interfaces is used to estimate $\widehat{a}\widehat{k}/G^{(2)}$. Each of the interfaces is formed by placing 50 micro-cracks over a period length of the interface. The lengths of the 50 micro-cracks are randomly generated to follow the $\chi^2(k)$ distribution ($k$ is a chosen positive integer), but the micro-cracks are positioned in such a way that the crack-tip gap is the same between any two consecutive neighboring micro-cracks. The crack-tip gap is related to $\widehat{a}$ and $\rho$ by $g = 2\widehat{a}(1-\rho)/\rho$.

For $\rho = 0.5$ and selected values of $G^{(1)}/G^{(2)}$, Figure 6 plots the non-dimensionalized effective stiffness $\widehat{a}\widehat{k}/G^{(2)}$ against $\widehat{h}$ for cases where the micro-crack length follows the $\chi^2(5)$, $\chi^2(10)$ and $\chi^2(25)$ distributions. The non-dimensionalized effective stiffness $a\widehat{k}/G^{(2)}$ calculated using the three-phase model is also plotted against $\widehat{h} = h/a$ in Figure 6. It is obvious that the non-dimensionalized effective stiffness of the micromechanical-statistical model becomes closer to that of the three-phase model if a larger degree of freedom is used in the $\chi^2$ distribution for generating the micro-crack length distribution. This is not surprising because the ratio of the standard deviation of the $\chi^2(k)$ distribution to the mean of the distribution is given by $\sqrt{2/k}$ and ap-

proaches zero as the degree of freedom $k$ increases (Abramowitz and Stegun [1]). Note the three-phase model assumes that every micro-crack has equal length and is evenly distributed along the interface. It is obvious that the three-phase model may not give a reliable estimate of the effective stiffness if there is a significant variation in the lengths of the micro-cracks on the interface.

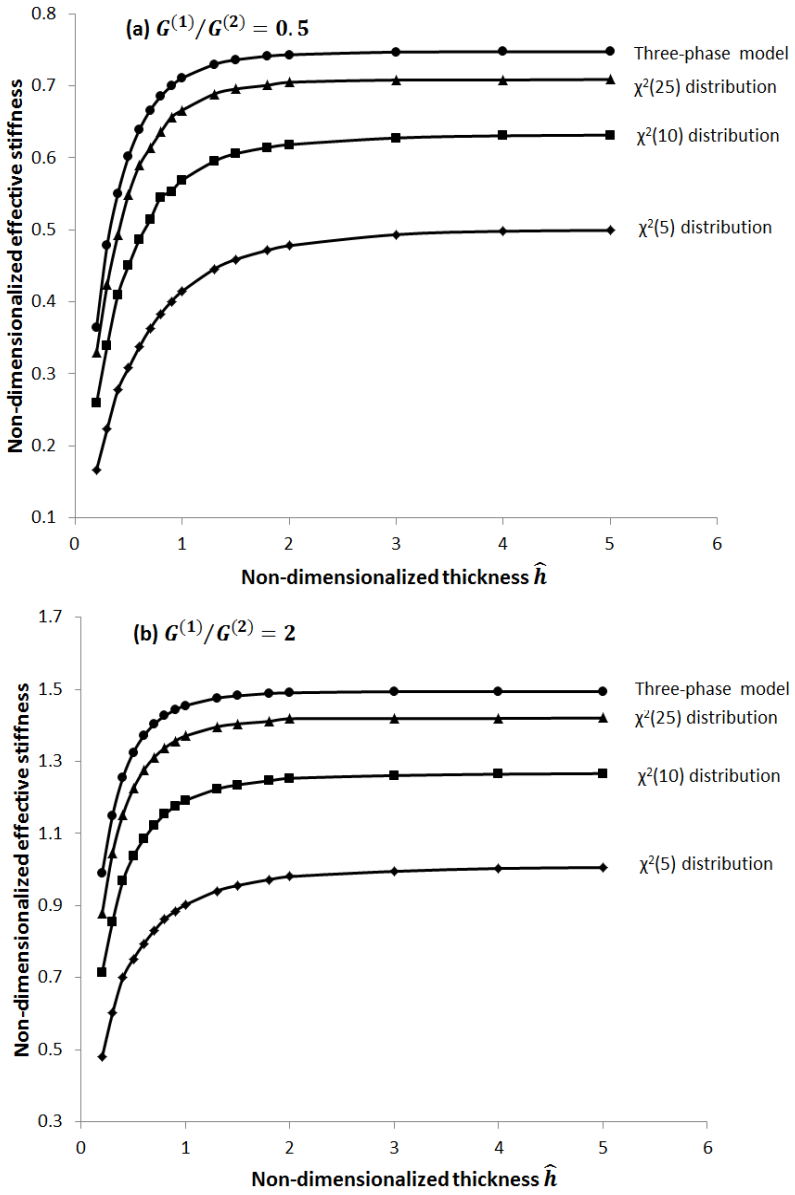


**Figure 6**. Plots of non-dimensionalized mean effective stiffness versus the non-dimensionalized thin layer thickness $\widehat{h}$, for lengths of micro-cracks generated by $\chi^2(5)$, $\chi^2(10)$ and $\chi^2(25)$ distributions. Also included are the corresponding values predicted by the three-phase model.

## 7.2 Number of micro-cracks for homogenizing the interface

The number of micro-cracks required on a period length of the interface for homogenizing the effective stiffness of the interface properly is examined here as follows. For fixed $G^{(1)}/G^{(2)}$, $\rho$ and $\widehat{h}$, a random sample of 50 interfaces is generated. Each interface contains $M$ micro-cracks over a period length of the interface. The lengths of the micro-cracks are chosen to follow the $\chi^2(k)$ distribution for a fixed $k$ and the $M$ micro-cracks are randomly positioned over a period length of the interface. If the number of micro-cracks needed to homogenize the interface is $M_0$, then the mean of the non-dimensionalized effective stiffness of the 50 interfaces (calculated as explained in Subsection 3.2) does not vary significantly with $M$ for $M \geq M_0$.

For $G^{(1)}/G^{(2)} = 1$, $\rho = 0.5$ and $\widehat{h} = 1$, the scattering and the means of the non-dimensionalized effective stiffness of the 50 interfaces generated by using the $\chi^2(5)$ distribution are shown in Figure 7 for various values of $M$. It is observed that the mean of the effective stiffness decreases dramatically as $M$ increases from 10 to 40 and it does not change significantly for $M$ exceeding 40. Furthermore, the range of the data for the effective stiffness of the 50 interfaces for $M = 40$ is narrower than that for $M = 10$. The range of the data does not seem to change very much for $M$ between 40 and 60. It appears that 40 micro-cracks per period length of the interface may be sufficient to homogenize the interface.

Further simulations are carried out using various other values for $\widehat{h}$, $G^{(1)}/G^{(2)}$, $\rho$ and $k$ show too that the observations above are true. In some cases, even 30 micro-cracks are found to be sufficient for homogenizing the

interface.

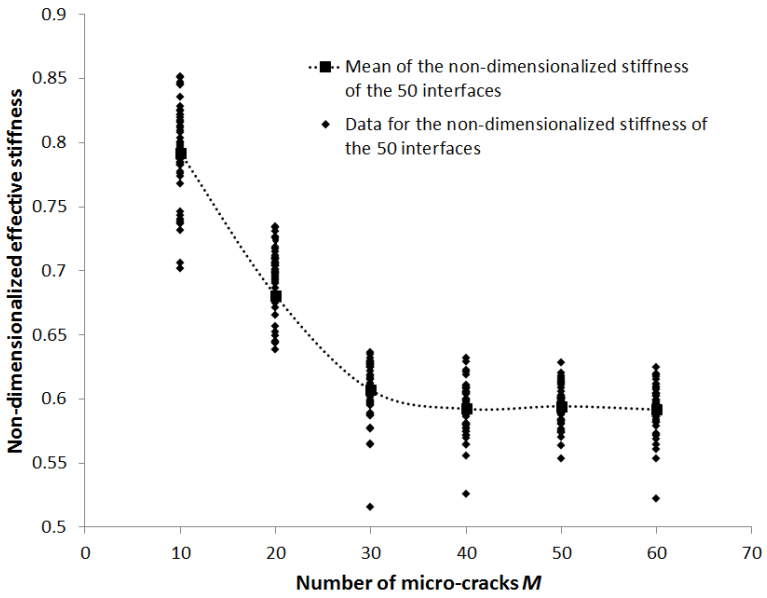


**Figure 7.** Scattering and means of the effective stiffness of the 50 interfaces for different $M$.

## 7.3 Some parametric investigations

To use the micromechanical-statistical model to conduct some parametric investigations on the effective stiffness of the interface, 50 interfaces are randomly generated for selected $\widehat{h}$ , $G^{(1)}/G^{(2)}$ and $\rho$. For each interface, the $\chi^2(5)$ distribution is used to generate the lengths of 40 micro-cracks which are randomly positioned on a period length of the interface.

Figure 8 plots the non-dimensionalized effective stiffness $\widehat{a}\widehat{k}/G^{(2)}$ against the damage ratio $\rho$ for selected values of $\widehat{h}$ and $G^{(1)}/G^{(2)}$. Three obvious trends are observed in Figure 8. Firstly, for fixed values of $\widehat{h}$ and $G^{(1)}/G^{(2)}$,

the non-dimensionalized effective stiffness of the interface decreases with increasing damage ratio $\rho$. This is not surprising as the micro-cracks occupy a larger portion of the interface, have smaller crack-tip gaps and tend to be less stable if the damage ratio $\rho$ is larger. Secondly, for fixed values of $\rho$ and $G^{(1)}/G^{(2)}$, the non-dimensionalized effective stiffness decreases as the non-dimensionalized thickness $\widehat{h}$ of the layer decreases. This is as expected as it is known that the plane boundary of the thin layer has the effect of making the micro-cracks less stable. Thirdly, for fixed values of $\rho$ and $\widehat{h}$, the non-dimensionalized effective stiffness increases with increasing $G^{(1)}/G^{(2)}$. This may be explained as follows $-$ coating the elastic half space with a layer of stronger material has the overall effect of strengthening the half space, thereby causing the micro-cracks to be more stable.

The non-dimensionalized effective stiffness is plotted against the non-dimensionalized thin layer thickness $\widehat{h}$ in Figure 9 for selected values of $\rho$ and $G^{(1)}/G^{(2)}$. For the values of $\rho$ and $G^{(1)}/G^{(2)}$ considered, the effective stiffness increases rapidly with increasing $\widehat{h}$ for $\widehat{h} < 1$, that is, if the thickness of the thin layer is less than the average half length of the micro-cracks. For $\widehat{h} > 1$, the effective stiffness increases slowly as $\widehat{h}$ increases and remains constant to within at least two significant figures for $\widehat{h}$ exceeding 4. Futher simulations show that the effective stiffness does not change significantly for $\widehat{h} = 10$, 100 and 1000. At least for $0.1 \leq G^{(1)}/G^{(2)} \leq 10$ and $0.1 \leq \rho \leq 0.9$, the analysis here seems to suggest that the plane boundary of the thin layer has hardly any effect in influencing the effective stiffness of the interface if the thickness of the thin layer is at least four times larger than the average half length of the micro-cracks.

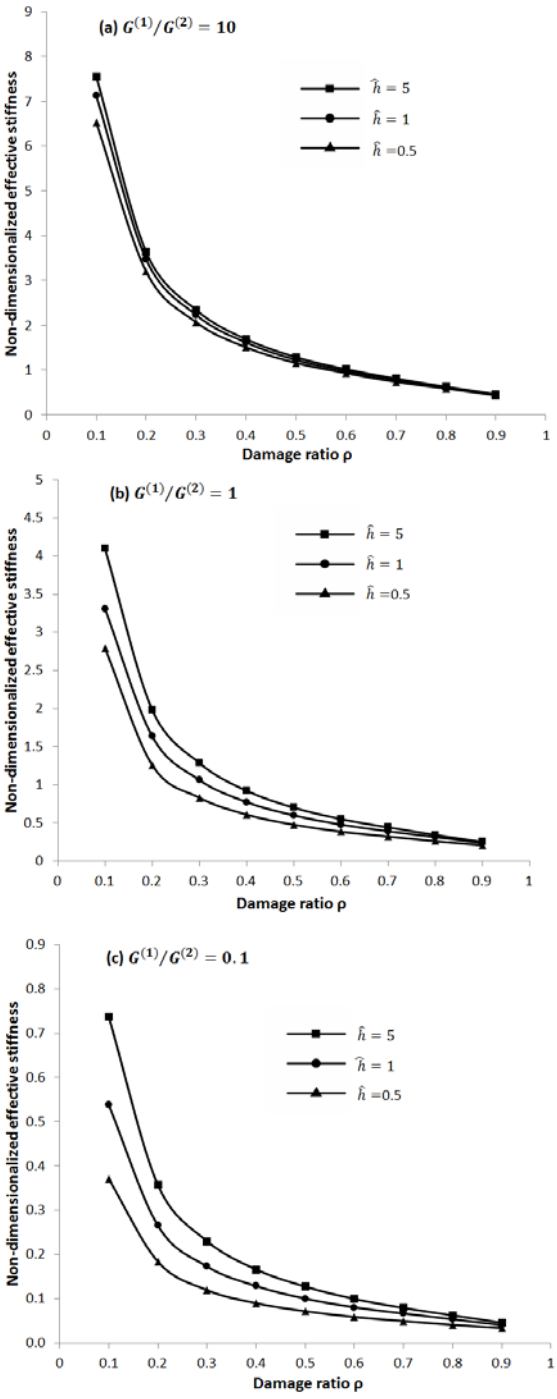


**Figure 8.** Plots of $\widehat{ak}/G^{(2)}$ against $\rho$ for selected values of $\widehat{h}$ and $G^{(1)}/G^{(2)}$.

To examine the effect of varying $G^{(1)}/G^{(2)}$ on the effective stiffness of the interface, the non-dimensionalized effective stiffness $\widehat{a}\widehat{k}/G^{(2)}$ is plotted against $\log_{10}(G^{(1)}/G^{(2)})$ in Figure 10 for $\rho = 0.5$ and selected values of $\widehat{h}$. For moderate values of $G^{(1)}/G^{(2)}$ within the range where $-1.5 < \log_{10}(G^{(1)}/G^{(2)}) < 2$, the plots for the different values of $\widehat{h}$ are visually distinguishable. As pointed out earlier, for a fixed $G^{(1)}/G^{(2)}$, the non-dimensionalized effective stiffness is larger for larger $\widehat{h}$. For $G^{(1)}/G^{(2)} > 100$, the non-dimensionalized effective stiffness increases very slowly as $G^{(1)}/G^{(2)}$ increases. At $G^{(1)}/G^{(2)} = 1000$, it converges to the same constant value of 1.41 (to within at least two significant figures) for all the three values of $\widehat{h}$ considered here. Thus, it appears that the plane boundary of the thin layer has negligible effect on the effective stiffness if the shear modulus $G^{(1)}$ of the thin layer is very much larger than the shear modulus $G^{(2)}$ of the half space. As $G^{(1)}/G^{(2)} \to 0^+$, the non-dimensionalized effective stiffness tends to zero no matter what $\widehat{h}$ is, that is, if the thin layer is extremely soft relative to the half space, the effective stiffness of the interface may be very small in magnitude.

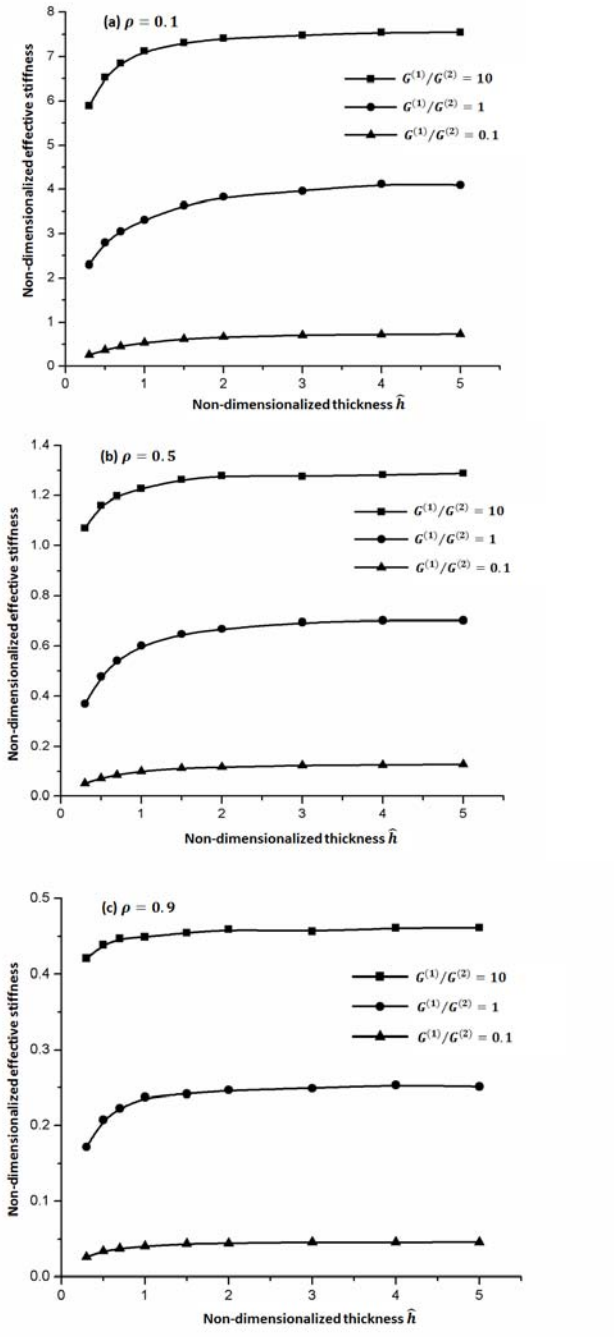


**Figure 9.** Plots of $\widehat{a}\widehat{k}/G^{(2)}$ against $\widehat{h}$ for selected values of $G^{(1)}/G^{(2)}$ and $\rho$.

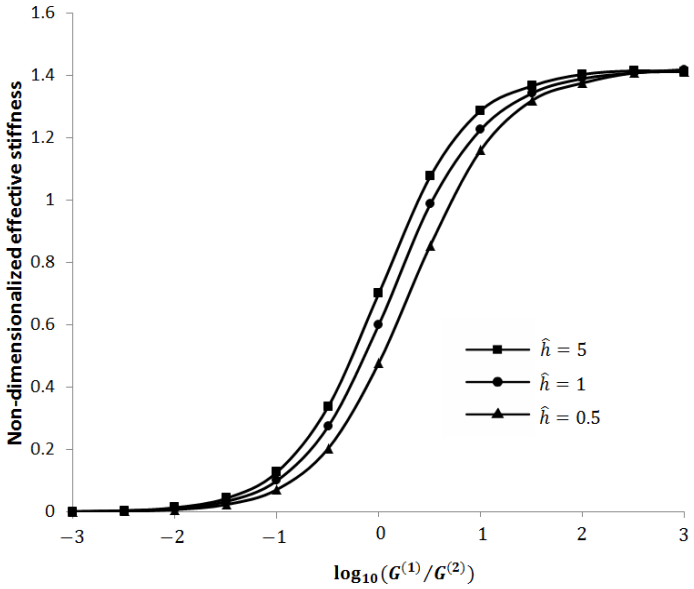


**Figure 10.** Plots of $\widehat{a}\widehat{k}/G^{(2)}$ against $\log_{10}(G^{(1)}/G^{(2)})$ for $\rho = 0.5$ and selected values of $\widehat{h}$.

# 8 Summary

Two different micromechanical models based on the hypersingular integral formulations are proposed here for the task of estimating the effective stiffness of a micro-cracked interface between an anisotropic thin elastic layer and an anisotropic elastic half space under antiplane deformations. The first model, which is called the three-phase model, simplifies the interface into three parts − micro-cracked, perfectly bonded and effective regions − which are periodically repeated along the whole interface. The second model known

as the micromechanical-statistical model, treats the interface as containing randomly positioned micro-cracks with statistically varying sizes.

The hypersingular integral formulations of both models are verified numerically by comparing the numerical procedures in Subsection 5.1 for three-phase model and Subsection 5.2 for the special case where the micro-cracks have equal length and are evenly distributed. As expected, the values of the effective stiffness of the interface computed by the numerical procedure in Subsection 5.1 are close to those by the numerical procedure in Subsection 5.2. For the values of thin layer thickness $\widehat{h}$ relative to the half micro-crack length, damage ratio $\rho$ and shear modulus ratio $G^{(1)}/G^{(2)}$ considered, the two sets of values agree to within less than $5\%$ – the agreement is better if the damage ratio $\rho$ of the interface is lower.

For simulations using the micromechanical-statistical model, the lengths of the micro-cracks are statistically generated based on a chosen $\chi^2$ distribution and the micro-cracks are randomly positioned. As expected, statistical simulations carried out using a $\chi^2$ distribution of a higher degree of freedom predict values of the effective stiffness closer to those given by the three-phase model. For the ranges of values used here for the shear modulus ratio $G^{(1)}/G^{(2)}$, damage ratio $\rho$ of the interface and the thickness $\widehat{h}$ of the thin layer relative to the average half micro-crack length, the number of micro-cracks required to homogenize the effective stiffness is around 40 micro-cracks per period length of the interface.

The micromechanical-statistical model is used to conduct some parametric studies on the effects of varying $\rho$, $\widehat{h}$ and $G^{(1)}/G^{(2)}$ on the effective stiffness of the interface. For fixed values of $\widehat{h}$ and $G^{(1)}/G^{(2)}$, the effective stiffness is a decreasing function of $\rho$. For fixed values of $\rho$ and $G^{(1)}/G^{(2)}$, the effective stiffness increases with $\widehat{h}$ but appears to tend to a constant as $\widehat{h}$ tend to infin-

ity. For a fixed non-zero $\widehat{h}$, the effect of the plane boundary on the effective stiffness is reduced as $G^{(1)}/G^{(2)}$ increases to an extremely large value, that is, as the thin layer becomes harder relative to the half space.

# References


[1] M. Abramowitz and I. Stegun, *Handbook of Mathematical Functions*, Dover, New York, 1970.

[2] W. T. Ang, *Hypersingular Integral Equations in Fracture Analysis,* Woodhead Publishing, Cambridge, 2013.

[3] Y. Benveniste and T. Miloh, Imperfect soft and stiff interfaces in two-dimensional elasticity, *Mechanics of Materials* **33** (2001) 309-323.

[4] J. R. Berger and A. Karageorghis, The method of fundamental solutions for heat conduction in layered materials. *International Journal for Numerical Methods in Engineering* **45** (1999) 1681-1694.

[5] D. L. Clements, *Boundary Value Problems Governed by Second Order Elliptic Systems*, Pitman, London, 1981.

[6] H. Fan and K. Y. Sze, A micro-mechanics model for imperfect interface in dielectric materials, *Mechanics of Materials* **33** (2001) 363-370.

[7] A. C. Kaya and F. Erdogan, On the solution of integral equations with strongly singular kernels, *Quarterly of Applied Mathematics* **45** (1987) 105-122.

[8] W. D. Nix, Mechanical properties of thin films, *Metallurgical Transactions A* **20** (1989) 2217-2245.

[9] Z. G. Suo and J. W. Hutchinson, Interface crack between two elastic layers, *International Journal of Fracture* **43** (1990) 1-18

[10] A. G. Varias, I. Mastorakos and E. C. Aifantis, Numerical simulation of interface crack in thin films, *International Journal of Fracture* **98** (1999) 195-207.

[11] X. Wang, W. T. Ang and H. Fan, Micro-mechanics models for an imperfect interface under anti-plane shear load: Hypersingular integral formulations, *Engineering Analysis with Boundary Elements* **36** (2012) 1856-1864.

[12] Y. Xu, J. A. Blume and C. F. Shih, An interface crack between an orthotropic thin film and substrate, *International Journal of Fracture* **63** (1993) 369-381